A tool for first order estimates and optimisation of dynamic storage resource capacity in saline aquifers.

Silvia De Simone*[ab] and Samuel Krevor[a]

[a] Imperial College London, Dept. of Earth Science and Engineering, London SW7 2AZ, UK

[b] Univ Rennes, CNRS, Géosciences Rennes - UMR 6118, Rennes, France

Abstract

The importance of carbon capture and storage in mitigating climate change has emerged from the results of techno-economic or integrated assessment modeling, in which scenarios of future energy systems are developed subject to constraints from economic growth and climate change targets. These models rarely include limits imposed by injectivity, ultimate amounts, or the geographic distribution of storage resources. However, they could if a sufficiently simple model were available. We develop a methodology for the fast assessment of the dynamic storage resource of a reservoir under different scenarios of well numbers and interwell distance. The approach combines the use of a single-well multiphase analytical solution and the superposition of pressure responses to evaluate the pressure buildup in a multiwell scenario. The injectivity is directly estimated by means of a nonlinear relationship between flow-rate and overpressure and by imposing a limiting overpressure, which is evaluated on the basis of the mechanical parameters for failure. The methodology is implemented within a tool, named CO2BLOCK, which can optimise site design for the numbers of wells and spacing between wells. Given its small computational expense, the methodology can be applied to a large number of sites within a region. We apply this to analyse the storage potential in the offshore of the UK. We estimate that 25-250 $GtCO_2$ can be safely stored over an injection time interval of 30 years. We also demonstrate the use of the tool in evaluating tradeoffs between infrastructure costs and maximising injectivity at two specific sites in the offshore UK.

[1]Corresponding author: Silvia De Simone, silviadesi@gmail.com

1 Introduction

Carbon capture and storage (CCS) is considered essential for mitigating climate change (IPCC, 2005). Several hundred Gt of CO_2 must be captured and permanently stored to achieve the net-zero CO_2 emission target by 2050 while approximately 220 $MtCO_2$ has been stored to date (IEA, 2017; IPCC, 2018; Global CCS Institute, 2017). The transition from megatonnes to gigatonnes of injected CO_2 requires the deployment of hundreds to thousands of large-scale projects with the commensurate potential for technical and economic limitations (Herzog, 2011). Emissions mitigation targets are estimated using a type of systems modelling known as techno economic or integrated assessment modeling (IPCC, 2018). These models rarely include limits imposed by the injectivity, ultimate amounts, or the geographic distribution of storage resources (Akimoto et al., 2004; Koelbl et al., 2014). However, these limitations can be accommodated by systems models should sufficiently simple models be developed to represent key aspects of CO_2 storage use.

There are different methods to estimate the amount of CO_2 that can be stored in a reservoir and the term ”storage capacity” often refers to different concepts (see Bachu, 2015, for a complete review and discussion). Volumetric estimates are based on the available pore space in the aquifer that may be filled with CO_2. These estimates are often classified as ”theoretical storage capacity” and they do not take into consideration constraints represented by the physical and chemical characteristics of the reservoir. Leading order limits on the use of subsurface saline aquifer resources may come from reservoir pressurisation, and plume migration towards leakage pathways (Szulczewski et al., 2012; Ringrose and Oldenburg, 2018). In practice, reservoir pressurisation is more often limiting over decadal timescales. With the exception of hydrocarbon reservoirs, reservoir pore space is already saturated by resident brine, and injected CO_2 leads to an increase in the pore pressure. This pressure build-up must be kept under certain limits to avoid reservoir fracturing, fault reactivation, or caprock failure, which can lead to felt seismicity, and in limited circumstances, CO_2 leakage from the reservoir (Bachu, 2008; National Academy of Science, 2012; Rutqvist et al., 2008; Rutqvist, 2012). Therefore, storage capacity should reflect the pressure-limited amount that can be safely stored and we adopt here this definition.

A number of simplified analytic models estimating the reservoir pressurisation have been developed and are potentially suitable for integration with techno-economic models (Neufeld et al., 2010; Krevor et al., 2019). The simplest involves approximation of the reservoir system as a closed volume and provides static estimates of pressure buildup based on the injected volume and compressibilities of rocks and fluids (Zhou et al., 2008). This is often overly conservative as it does not take into consideration the temporal evolution of the storage capacity and the permeability of reservoir bounding lithology which can serve as a pressure relief (Vilarrasa and Carrera, 2015). More accurate estimates are provided by models capturing the dynamic nature of both plume migration and reservoir pressurisation in response to the time evolution of storage resource use (Nordbotten et al., 2005; Dentz and Tartakovsky, 2009; Mathias et al., 2009, 2011; Vilarrasa et al., 2010; Azizi and Cinar, 2013). These models solve the governing multiphase flow equations for a problem geometry in which there is a single injection well in a reservoir. These single-well models have been extended to estimates of pressurisation during simultaneous injection through multiple wells by superposing their solutions (Ganjdanesh and Hosseini, 2017; Huang et al., 2014; Joshi et al., 2016; Zakrisson et al., 2008). While not mathematically rigorous, De Simone et al. (2019) show that the error in the use of superposition is small for a wide range of injection scenarios relevant to the development of regional subsurface storage resources, and a correction factor may be applied in the case in which the error is significant.

This approximation allows for a consideration of the kinds of tradeoffs that may arise in the comparison of scenarios considered in energy systems models. For example, on the one hand, using multiple injectors may increase the reservoir injectivity, although this is highly dependent on factors such as reservoir pressure, injection rates, and spacing between wells. On the other hand, the construction and operation of wells is a significant contributor to investment and operating costs, and may not always be justified by the increased volume of CO_2 that may be stored.

In this paper we build on the analysis in De Simone et al. (2019) to develop a methodology to estimate CO_2 injection rates that maximise storage whilst not exceeding a limiting pore pressure increase specific of the reservoir. A range of scenarios of injection well number and inter-well distance is explored. The methodology has been implemented within an open source software tool named CO2BLOCK. The computational expense of the estimation is of the order of seconds in a normal desktop machine, which allows for an optimisation of well numbers and spacing around an objective of interest such as storage capacity or net revenue. We demonstrate two applications in the UK offshore system: estimates and sensitivity analysis of the total storage resource of the offshore UK, and a net revenue estimate which incorporates tradeoffs between injectivity and capital costs associated with injection wells for site buildout at two specific sites.

2 Methodology

The tool, which is named CO2BLOCK, estimates the maximum rate of injection and ultimate storage resource of a reservoir in which CO_2 is injected into a number n of vertical wells on a geometrical grid with spacing d. This is done for a range of n and d such that the output can be used as a basis for further optimisation. Overpressure, i.e., the pore pressure increase with respect to the initial conditions, is assumed as the major constraint and it must be kept below a critical value. We define the storage capacity as the maximum amount that can be stored without exceeding the critical overpressure. The reservoir is assumed as homogeneous, with the wells placed on a Cartesian grid and all operating with the same injection rate, which is constant in time.

The workflow follows four steps following the input of data (Figure 1). First, the maximum sustainable overpressure in the reservoir is estimated according to the initial conditions and the mechanical conditions for failure. Second, the tool predicts the pressure increase in response to a reference CO_2 injection flow-rate. Third, the maximum sustainable injection rate is estimated for the range of scenarios of well number and spacing by ensuring that the maximum allowable overpressure is not exceeded. Fourth, three further constraints, related to technical limitations and reservoir dimension, eliminate a number of scenarios. From this information, scenarios may be identified according to defined optimization criteria, such as storage maximising scenarios, or revenue maximising scenarios. We provide an overview in the following, while further details are provided in Supporting Information.

The methodology is first applied to an illustrative example whose characteristics are detailed in Table 1. For the example case, the maximum interwell distance is set to 10 km and the maximum well number to 42 (a 6×7 grid). All properties are considered uniform over the reservoir and constant in time. Initial pressure and temperature, brine and CO_2 properties, and geomechanical parameters may be provided as input, with values spanning over the typical ranges. If not provided, default values are assumed for compressibility and geomechanical properties, while fluid properties are calculated according to equations of state (see Table S3 in Supporting Information).

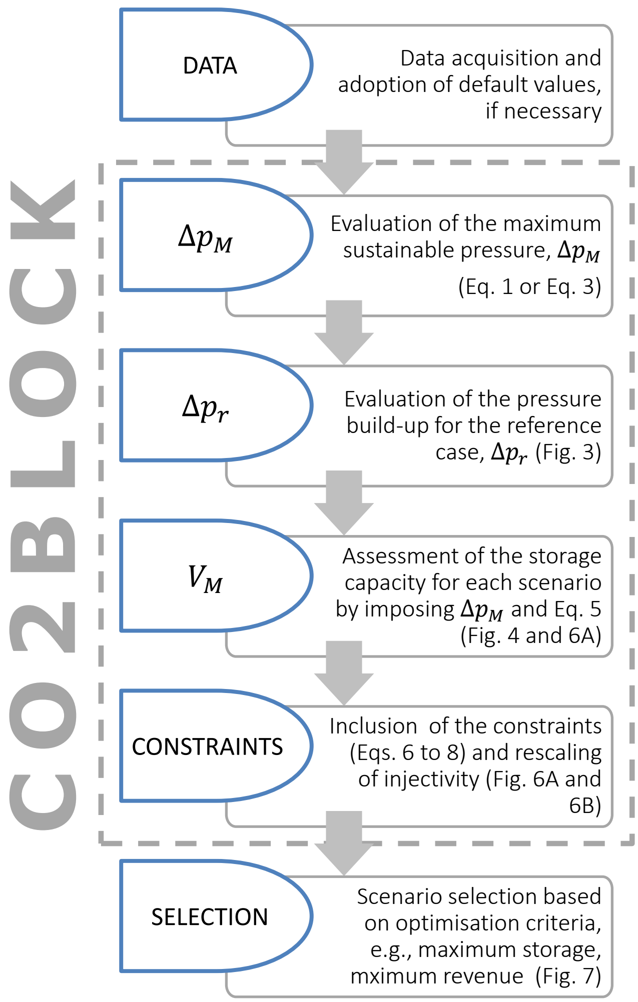

Figure 1: Methodology for the assessment and optimization of the CO_2 storage capacity using CO2BLOCK. Steps enclosed in the dashed rectangle are the steps taken within CO2BLOCK. Further details are provided in Supporting Information, Section S7.

Table 1: Parameters adopted for the case example.

Symbol	Parameter	Value	Units
Input parameters			
A	Reservoir surface area	900	km^2
BC	Domain boundary type	open	-
c_r	Rock compressibility	1×10^{-10}	Pa^{-1}
c_w	Brine compressibility	1×10^{-10}	Pa^{-1}
C	Cohesion	0	MPa
H	Thickness	250	m
k_0	Stress ratio	0.5	-
p_0	Initial pressure	15	MPa
Q_r^{tot}	Reference total injection rate	10	Mt/yr
Q_s	Technical limit to injection rate per well	2	Mt/yr
r_w	Well radius	0.05	m
S_0	Tensile strength	0	MPa
t	Injection time	40	yr
ζ_m	Average depth	1500	m
κ	Permeability	5×10^{-14}	m^2
μ_w	Brine viscosity	5×10^{-4}	Pa s
μ_c	CO_2 viscosity	5×10^{-5}	Pa s
ρ_c	CO_2 density	900	kg/m^3
σ_1	Maximum principal stress	40.5	MPa
ϕ	Porosity	0.2	-
φ	Friction angle	27	$^\circ$
Output parameters			
p_M	Maximum sustainable pressure		MPa
Q_M	Maximum sustainable injection rate per well		Mt/yr
V_M	Maximum storage capacity		Gt

2.1 Limits to pressure build-up

A major technical constraint to storage comes from the geomechanical response of the reservoir to the pressure increase. The possibility of activating pre-existing faults or opening new fractures is an issue of great concern, primarily due to seismicity, but also due to the potential for CO_2 leakage back to the atmosphere (Zoback and Gorelick, 2012; Vilarrasa and Carrera, 2015; Ellsworth, 2013; National Academy of Science, 2012).

Rock failure may occur in either a tensile or shear mode (Jaeger et al., 2009). Tensile failure is likely to occur along planes normal to the minimum principal stress, σ_3, when the pore pressure is greater than the sum of σ_3 and the rock tensile strength, S_0. The limiting pressure build-up for tensile failure, Δp_M^t, is given by

$$\Delta p_M^t = \sigma_3 - p_0 + S_0 \,, \tag{1}$$

where p_0 is the initial pressure, often assumed equal to the hydrostatic pressure. It is common practice to assume $S_0 = 0$, which means that the fracture pressure is equal to the minimum principal stress.

Shear failure occurs along a given orientation when the shear stress, τ, overcomes the frictional forces, according to the Mohr-Coulomb failure criterion

$$\tau - [C + (\sigma_n - p) \tan \varphi] \geq 0 \,, \tag{2}$$

where σ_n represents the stress acting normal to the orientation, φ is the internal friction angle, and C is cohesion, which many experimental data show to be often equal to $2S_0$ (Jaeger et al., 2009). By assuming that failure occurs along the most critical orientations (i.e., the ones forming angles of $(\pi/4 \pm \varphi/2)^\circ$ with the direction of the maximum principal stress, σ_1), the limiting pressure build-up for shear mode, Δp_M^s, can be expressed by

$$\Delta p_M^s = \frac{k_0 - \theta}{1 - \theta}(\sigma_1 - p_0) + C\frac{\cos\varphi}{\sin\varphi} \,, \tag{3}$$

where $k_0 \leq 1$ is the ratio between the minimum and the maximum principal effective stresses, i.e., $k_0 = \sigma_3'/\sigma_1' = (\sigma_3 - p_0)/(\sigma_1 - p_0)$, while $\theta = (1 - \sin\varphi)/(1 + \sin\varphi)$. The conservative assumption of $C = 0$ acknowledges that shear failure is likely to occur along planes of weakness, e.g., faults.

The difference between equations (1) and (3) indicates which of the two overpressure limits will be exceeded first,

$$\beta = \Delta p_M^t - \Delta p_M^s = \left(k_0 - \frac{k_0 - \theta}{1 - \theta}\right)(\sigma_1 - p_0) + S_0 - C\frac{\cos\varphi}{\sin\varphi}. \tag{4}$$

Positive values of β indicates that shear failure is more likely to occur than tensile failure and vice-versa. In the case of cohesionless rocks ($C = S_0 = 0$), failure mostly occurs in shear mode ($\beta > 0$), regardless of the stress conditions, since the first term on the right hand side of Equation (4) is always positive (Figs. 2A and C). Conversely, in the case of cohesive rocks, tensile failure is more likely to occur ($\beta < 0$) at shallow depths, where the effective stresses are smaller, even for small values of S_0 (Figs. 2B and D). This explains the processes of hydrofracturing performed in unconventional gas exploitation, where tensile failure is activated at depths less than 3 km in shale rocks with S_0 between 5 and 10 MPa (Chandler et al., 2016; Peduzzi and Harding Rohr Reis, 2013).

In our methodology the maximum sustainable overpressure, Δp_M, is evaluated as the lower value of the tensile and shear failure pressures, Δp_M^t and Δp_M^s. This evaluation is complicated by the uncertainty in the parameter values and by the reservoir heterogeneity. The relative magnitude and the orientation of the principal stresses defines the planes that are more likely to fail, as well as the critical overpressure. However, the *in situ* confining stress is often unknown. A common practice is to assume that one of the principal stresses is the vertical stress and is given by the lithostatic pressure. The other two principal stresses are therefore horizontal and can be estimated by the observations of wellbore compressive (breakouts) and tensile (drilling- induced) failures (Zoback et al., 2003). The lack of these

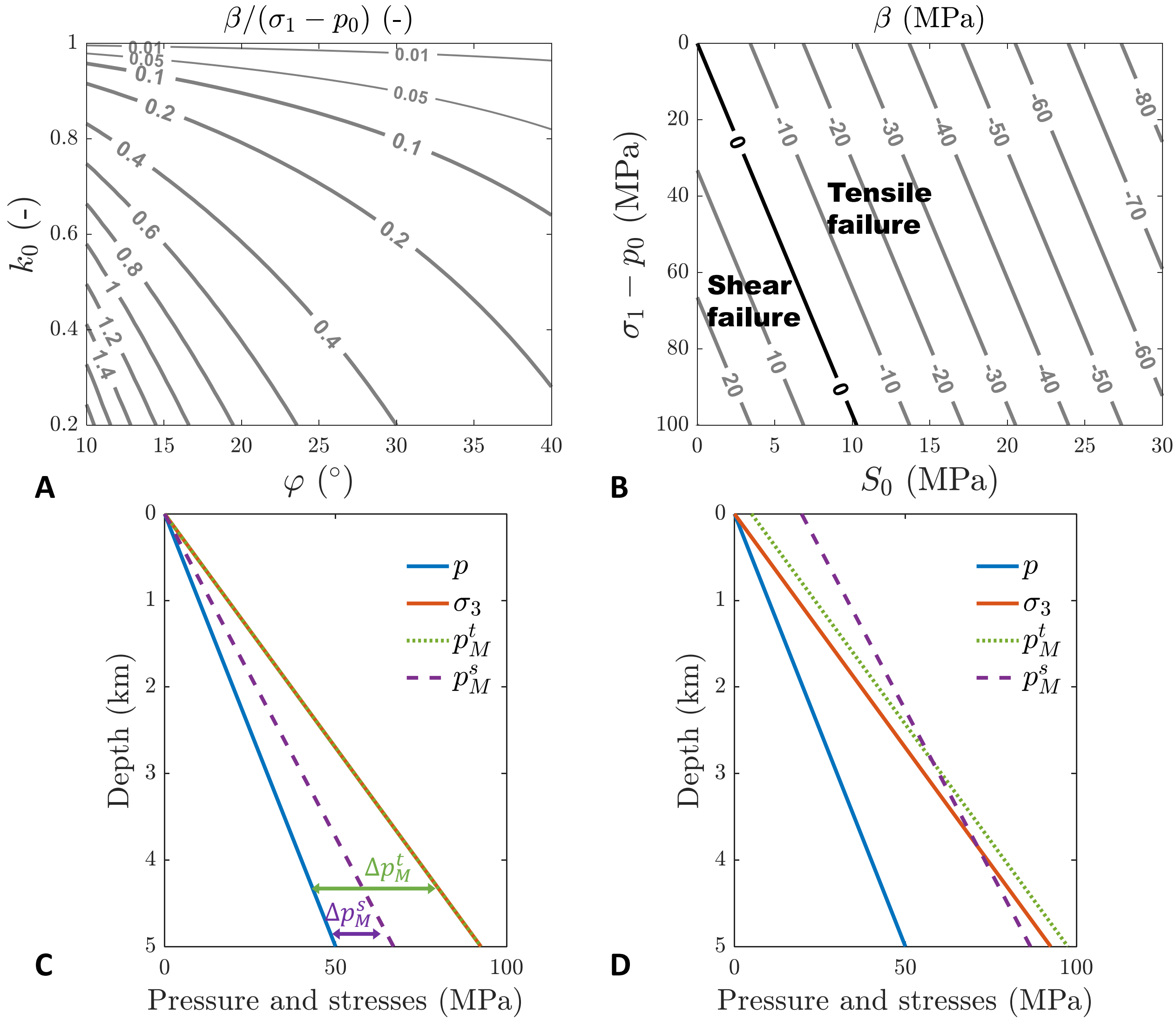

Figure 2: Example of potential for tensile and shear failure under different scenarios for cohesionless (left) and cohesive rocks (right). **A**: For cohesionless rock ($C = S_0 = 0$), the factor $\beta/(\sigma_1 - p_0)$ (eq. (4)) changes with the stress ratio k_0 and the internal friction angle φ, but it is always positive, which indicate that shear failure is more likely to occur over tensile failure. **B**: For cohesive rocks the values of β indicate that the failure mode is a function of the confining stress ($\sigma_1 - p_0$), as well as of the other parameters. In the example here, $C = 2S_0$, $\varphi = 27°$ and $k_0 = 0.5$. **C and D**: Variation of pressure and pressure limits with depth for cohesionless and cohesive rocks, respectively. We assume that σ_1 is the vertical stress and that $\varphi = 27°$ and $k_0 = 0.5$. Cohesion is $C = 2S_0 = 10$ MPa in the case of cohesive rock. Notice that the limiting pressure for tensile failure p_M^t coincides with σ_3 in the case of cohesionless rocks and it is greater than the limiting pressure for shear failure p_M^s for any depth. For cohesive rocks, the potential for tensile failure is greater than for shear failure at shallow depths (i.e., $p_M^t < p_M^s$), but the trend inverts for greater depths.

data generates large uncertainties in the evaluation of the pressure limit. Moreover, the presence of heterogeneity and planes of weakness is difficult to detect. We show how uncertainties in input data may be evaluated in the applications in Section 3.1.

2.2 Pressure build-up for a reference injection rate

The next step is the prediction of the pressure buildup in response to a reference CO_2 injection rate, over a specified time interval. This will be later used in the calculation of a maximum possible injection rate, subject to constraints. Pressurisation is evaluated according to an approach developed in De Simone et al. (2019). In summary, we adopt the solution to single well CO_2 injection proposed by Nordbotten et al. (2005) with a modified version for closed boundary domains (see Supporting Information, Section S1). The response to the simultaneous CO_2 injection into multiple sites at a specified constant rate is estimated as the superposition of single-well solutions, evaluated at the inner-most well, where the overpressure is highest. The use of the superposition in the case of multiphase flow results in an overestimate of the overpressure. The error is small for less than nine wells but becomes significant with an increasing number of wells. With greater than nine wells, a correction factor can be used to improve the estimate (supporting information, Section S3). This option is available in the software tool that we provide but it is not used in the examples shown here such that error is always in the direction of an overestimation of the pressure buildup, corresponding to conservative estimates of CO_2 storage volumes.

The use of this approach allows us to evaluate various scenarios of well numbers and interwell spacing for a total given injection rate into a reservoir unit. Figure 3 shows the response to a reference total flow rate of $Q_r^{tot} = 10$ Mt yr^{-1} for 40 years in the case example reservoir (Table 1). The pressure buildup decreases by increasing the number of wells and increasing the distance between wells, but the response is non-linear. This allows for site design subject to the constraint of maintaining pressure below the critical value, Δp_M.

2.3 Estimating the maximum flow rate

The pressure response to the reference injection rate can be used to estimate the maximum sustainable flow rate, Q_M. This rate leads to a calculation of the maximum amount of CO_2 that can be continuously stored in a time interval, t, without exceeding the pressure limit, Δp_M. In the case of single phase flow, the pressure build-up, Δp, increases linearly with the injected flow rate, Q. Some authors have extended the linearity of the $\Delta p/Q$ relationship to the case of multiphase flow (Szulczewski et al., 2012; Zhou and Birkholzer, 2011). This allows them to estimate the maximum sustainable flow rate as $Q_M(t) = Q_r \Delta p_M / \Delta p_r(t)$, where Δp_r is the pressure response to the injection of a reference flow rate Q_r, estimated at the inner-most well. However, the nonlinearity of multiphase flow makes this approximation valid only for small variations of flow rate, i.e., $Q_M \approx Q_r$.

For greater variations of Q, the variation of overpressure is strongly nonlinear, especially for open domains and a small number of wells (Fig. 4, Supporting information Figs. S1 and S2). This can give raise to significant errors in the estimation of the storage capacity. If the

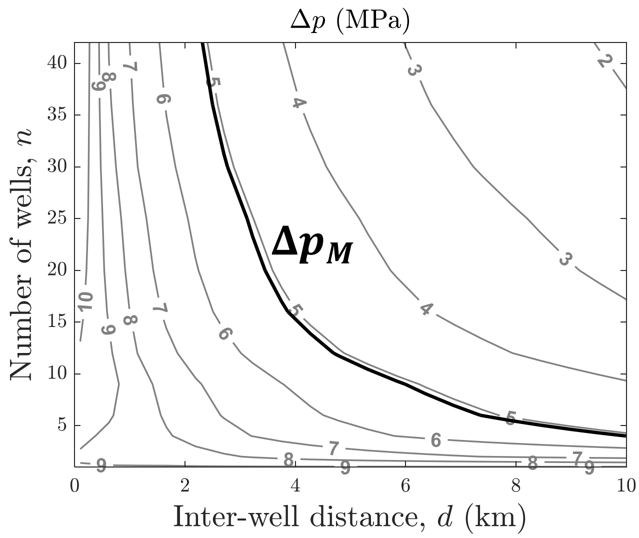

Figure 3: Pressure build-up at the inner-most well of the case example reservoir in response to 40 years of continuous injection under different scenarios of well number and spacing. The estimate is performed by superposition of single-well analytical solutions. The black solid line represents the maximum sustainable overpressure.

reference flow rate, Q_r, is smaller than the actual injectivity, Q_M, the linear assumption leads to an underestimate of the storage capacity. The adoption of a reference flow rate greater than the injectivity overestimates the storage capacity (Fig. 5).

We derive the exact relationship between overpressure and flow rate valid for both single and multiwell cases (Fig. 5 and Supporting Information, Section S2). This allows for the direct calculation of the maximum flow rate, given the overpressure response in a reference scenario,

$$Q_M(t) = -\frac{Q_r \widetilde{\Delta p_M}}{W\left(-\widetilde{\Delta p_M}\exp(-\widetilde{\Delta p_r(t)})\right)}, \tag{5}$$

where both the reference and the maximum sustainable flow rates refer to the mass injection into each well, $\widetilde{\Delta p_y} = \Delta p_y/(bQ_r)$, $b = (\mu_w - \mu_c)/(4\pi\kappa H\rho_c)$, κ is the absolute permeability, H is the reservoir thickness, ρ_c is the CO_2 density, μ_w and μ_c are the brine and CO_2 dynamic viscosities, respectively, while $W(x)$ represents the Lambert function for $x < 0$. This direct estimation provides a rapid assessment of the maximum sustainable flow rate for a number of scenarios (Fig. 6A). Note that density and viscosity are considered as constant during the injection. However, for both CO_2 and brine, density and viscosity increase with increasing pressure, especially in the case of CO_2. Considering this variation would introduce an additional non-linearity in the relationship between overpressure and injected flow rate.

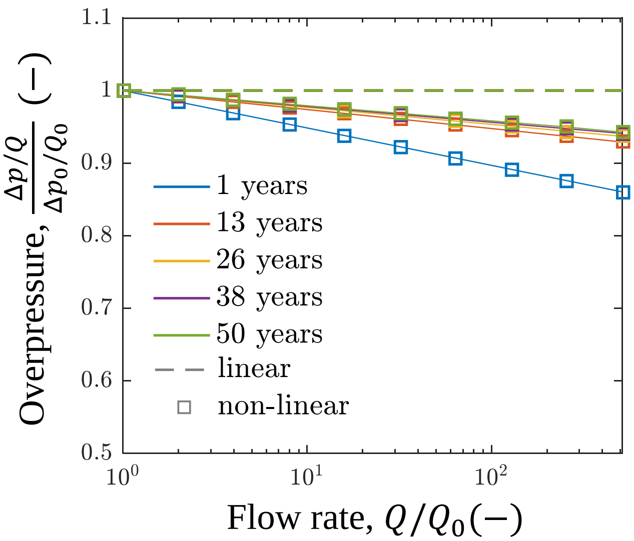

Figure 4: Maximum overpressure response normalized with respect to the injected flow rate under different flow rates of CO_2 injection. Values are non-dimensionalised with respect to the case of the smallest injection rate, Q_0. Pressure build-up is evaluated at the inner-most well of the case example for the 16 wells scenario with interwell distance equal to 2 km. Colours correspond to different injection times (from 1 up to 50 years). Solid lines correspond to the solution calculated for each injection rate. Dashed lines, which all fall on the same line, represent the extrapolation of the pressure build-up from the response to Q_0, by assuming a linear $\Delta p/Q$ relationship. Markers represent the extrapolation by means of the non-linear $\Delta p/Q$ relationship (see Eq. (S5) in Supporting Information). Note that the plot is represented in semi-log scale.

2.4 Constraints imposed by plume migration, reservoir dimension, and technical limitations to well injection rates

There are two constraints, a lower and upper, on the interwell distance. The first comes from the need to avoid CO_2 plume interference. This defines a lower constraint such that the half of the interwell distance is smaller than the plume average propagation distance, which gives

$$d > 2\sqrt{\frac{Q_M t}{n\pi\phi H\rho_c}}. \tag{6}$$

Note that plume intersection does not affect storage feasibility or safety. In this study, avoiding plume interference is a condition related with the assumptions underlying the adopted analytical model (see also section S1 and S2 in Supporting Information). Allowing plume interference would possibly imply a modification of the analytical solution and a verification/update of the error correction factor, which will be subject of future work and development of CO2BLOCK.

An upper constraint is defined by the reservoir surface area A, which limits the number of wells at a given spacing. Assuming that the well distribution is a Cartesian grid, and assuming a buffer area on the outer perimeter equal to $d/2$, the constraints imposed by the

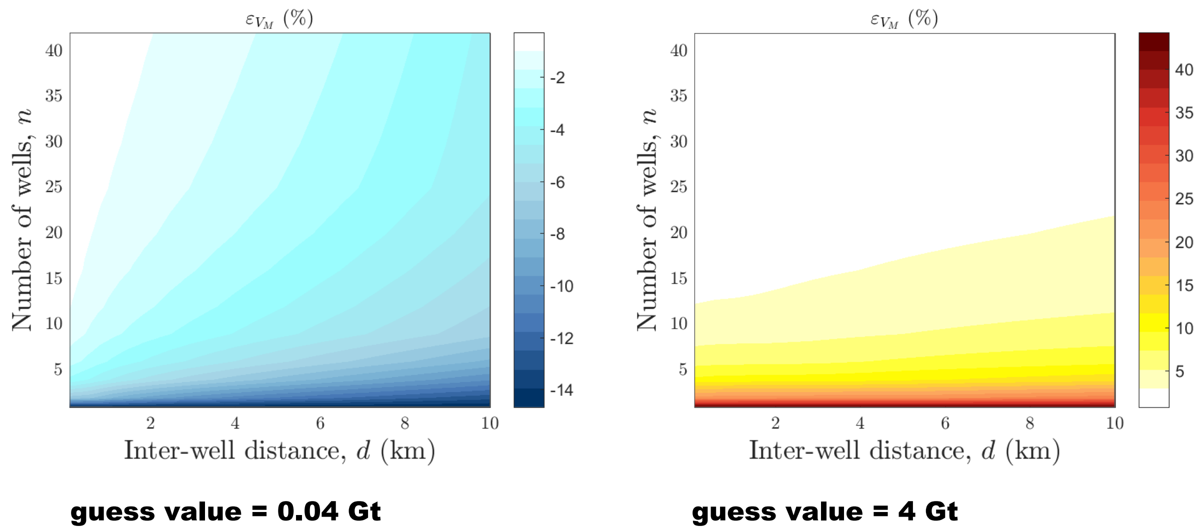

Figure 5: Relative error associated with the adoption of a linear $\Delta p/Q$ relationship for different well configurations of the case example adopted here, whose maximum storage capacity, V_M, is between 0.2 and 1.1 Gt for a 40 years injection (Fig. 6A). The linear approximation underestimates the storage capacity V_M if a small reference value is adopted (left), while it overestimates V_M if a greater reference value is assumed (right). The error is particularly high for small number of wells, according to the nonlinearity effects.

areal size of the reservoir is given by

$$d \leq \sqrt{A/n}. \tag{7}$$

There are technical limitations to the injectable flow rate per well and this is reflected by setting a value, Q_s, such that.

$$n \geq Q_M^{tot}/Q_s, \tag{8}$$

where Q_M^{tot} is the total injection rate, the sum of injection through the n wells. The storage resource use scenarios before and after these constraints are imposed are shown in Fig. 6A and Fig. 6B, respectively.

2.5 Optimising storage design

There are a number of ways in which storage resource use might be optimised. In Figure 7 we estimate the maximum storage achievable in the reservoir for all scenarios of injection well numbers. Figure 7 shows that the maximum capacity does not necessarily correspond to the maximum number of wells. For this location, there is a maximum storage resource use obtained with the deployment of 20 wells throughout the formation. It is notable that in this example the storage capacity increases with the well number until reaching a sort of plateau, which corresponds to scenarios in which the storage is constraint by the reservoir surface area (observe the red line in Fig. 6B). Therefore, nearly the same capacity can be achieved with 16 wells, possibly presenting greater value for money. In the following sections

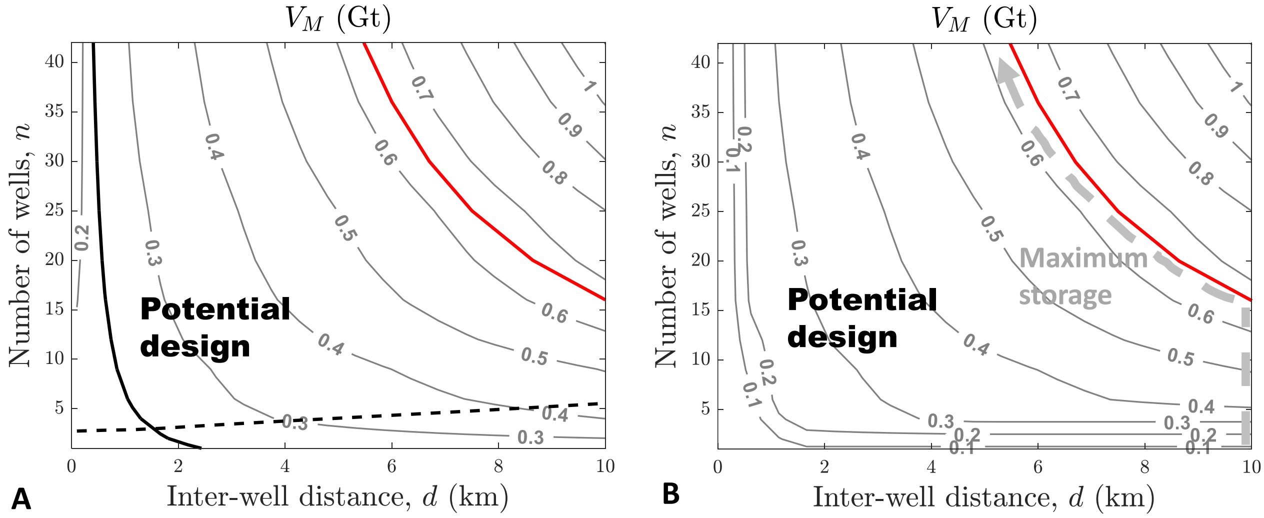

Figure 6: CO_2 storage capacity for the case example under different scenarios of well number and spacing and with 40 years of injection. **A**: pressure-limited storage capacity according to Eq. (5) and imposing the maximum sustainable pressure, Δp_M. The black solid line represents the lower constraint to avoid plume interference (Eq. (6), the black dashed lines represents the lower constraints associated with technological limits (Eq. (8)), while the red solid line represents the upper constraint imposed by the reservoir dimension (Eq. (7)). **B**: Plausible storage capacity after the scaling out of those values of injectivity that fall out of the lower constraints (black solid and dashed lines in Fig. A). The dashed grey arrow defines the scenarios of maximum storage capacity, shown in Fig. 7.

we apply the tool for two targets - the assessment of the dynamic storage capacity of UK reservoirs, and optimising the use of specific reservoirs for maximum revenue.

3 Applications

3.1 Dynamic Storage Resources of the UK

We apply the methodology described in Section 2 (Fig. 1) to assess the maximum potential for CO_2 storage in the UK offshore system. All data have been collected from the CO_2 stored database (Bentham et al., 2014; Energy Technologies Institute LLP, 2018), which contains information including geological data for nearly 600 potential CO_2 storage units located offshore UK. These include oil and gas reservoirs and saline aquifers.

We perform an initial screening to identify a subset of the sites with the most beneficial attributes for storage. Our analysis is limited to saline aquifers, representing about the 85% of the total storage capacity in the UK (Gammer et al., 2011; Pale Blue Dot Energy, 2016). The analysis is further restricted to formations where the caprock is deeper than 1 km in the subsurface, to ensure CO_2 remains in a supercritical state (IPCC, 2005). Only sites with permeability greater than 1 mD and porosity greater than 0.1 are considered. Finally, the aquifers with theoretical CO_2 storage less than 200 Mt are excluded. The screening reduces

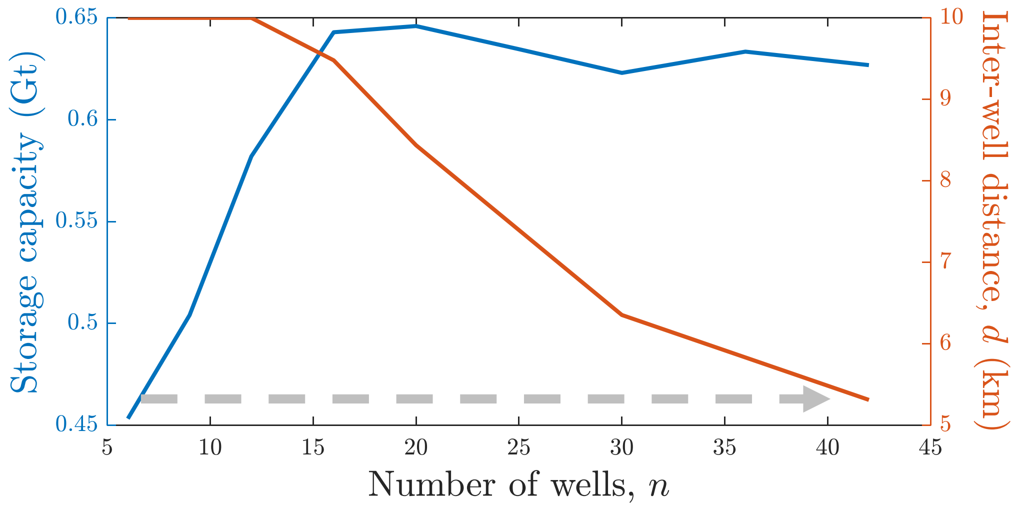

Figure 7: Maximum storage capacity for the case example for each scenario of well number (corresponding to the dashed grey arrow in Fig. 6B). The corresponding well spacing is represented by the orange line.

the consideration from 292 potential saline aquifer sites to 25, mostly located in the Northern, Southern or Central North Sea (see inset of Fig. 9 and Section S4 in supporting information for further details). They represent approximately 1/3 of the total theoretical capacity of 60 Gt provided by the 292 saline aquifers.

The database does not provide information about the *in situ* stress conditions and the mechanical parameters, which are essential for the evaluation of the maximum sustainable pressure. We assume that the maximum stress is the vertical stress, σ_v, which implies that the minimum stress is horizontal, σ_h. For the mechanical parameters, we adopt the values detailed in Table S3 of Supporting Information. A sensitivity analysis for these parameters is performed in the following. We set the technical limit to injectable flow rate per well, Q_s, to 5 Mt yr^{-1} and we assume continuous injection for 30 years.

Figure 8 shows the injectivity for two of the most significant sites as examples. The Forties 5 has a very large area and open boundaries, which allows for the injection of huge flow rates without exceeding the critical pressure. However, the absence of structural confinement may lead to lateral migration of CO_2 (Bentham et al., 2014). For less than 10 injectors placed at large distance (see inset of the left panel), the cut-off constraint is represented by the maximum technological capacity of injection Q_s, which means that even greater flow rate might be injected in the case of further technological improvements. For larger number of injectors, plausible scenarios are limited by the reservoir surface area, i.e., the combination of well number and distance must be such that the well pad size does not exceed the reservoir surface area (eq. (7)). The maximum per well injectivity reduces with increasing number of injectors (scenarios close to the red line). This reduction is however compensated by the increasing number of injectors, resulting in a roughly constant storage capacity when the well number is greater than 200 (see Fig. S3A and B in Supporting Information). The Bunter Closure 28, as well as the other Bunter closures, are stratigraphic traps with relatively small volumes. However, the trapping topography makes them promising sites for storage. As a consequence of the closed boundaries and the small surface area, increasing the well number does not compensate the reduction in the per well injectivity, thus storage is maximized with few injectors placed at large distance (see also Fig. S4A and B in Supporting Information).

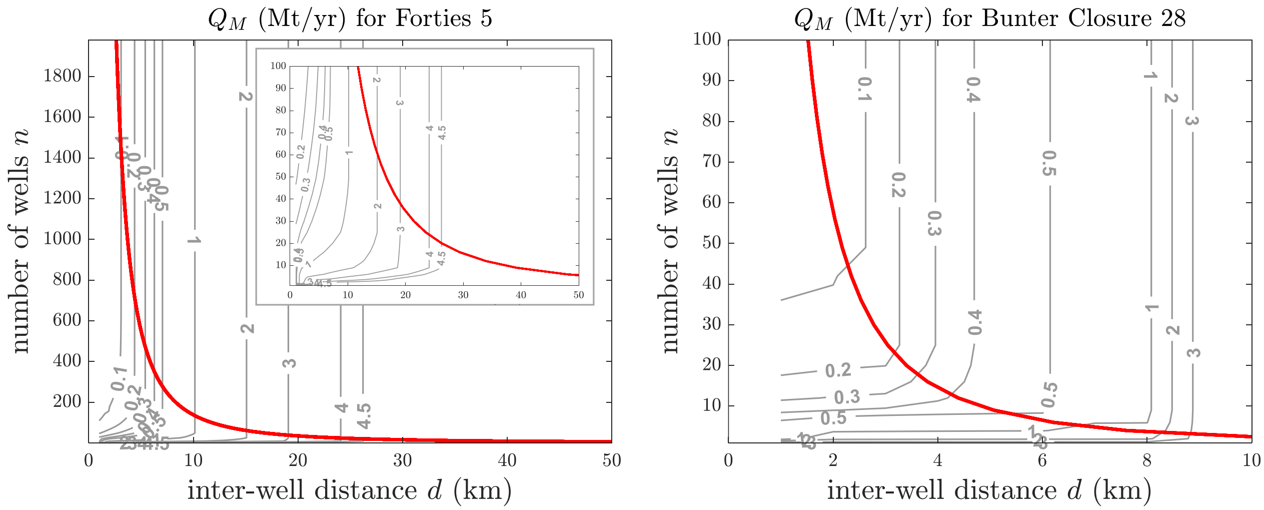

Figure 8: Examples of the per well injectivity estimated for an open (left) and a closed (right) reservoir. Contours show the maximum sustainable flow rate per well for 30 years of injection. The red lines show upper limits imposed by the reservoir area, i.e., plausible scenarios are to the left of the red lines. See text for further details.

For the Forties 5 the maximum storage is achieved with a very large number of wells (around 1300, see Fig. S3B in Supporting Information), which may be unfeasible due to other practical limitations not considered by the tool. However, for reservoirs with these characteristics (large reservoirs with open boundaries), the storage capacity is essentially constrained by the reservoir surface area, thus it becomes approximately constant for well numbers greater than a certain value, and the maximum storage estimate may reflect a local maximum. We thus limit the well number to 200, but we also analyze the cases with maximum well number equal to 2000 and 50.

Figure 9 shows the total mass that can be stored in the UK reservoir system over a period of 30 years. Numerical values and corresponding scenarios are detailed in Table 2. The total storage capacity provided by the 25 selected sites is approximately 140 Gt over 30 years, which corresponds to a total injection rate of 4.7 Gt yr^{-1}. If the maximum well number is capped at 2000, then the storage mass is 165.5 Gt, while if the well number is limited to 50, the storage resource is reduced to 68 Gt (see Table S1 in Supporting Information). This reflects that the storage capacity is approximate constant for $n > 200$ for most reservoirs in this example.

The greatest storage resource is provided by the Mey 5, Maureen 2 and several Cormorant sites, each providing more than 10 Gt of storage. These sites reveal the huge storage resource potential of the Central and Northern North Sea. A similar storage capacity is provided by the Collyhurst formation in the East Irish Sea. Note that for some of these sites the storage capacity is capped by the maximum number of wells, i.e., they are not pressure limited in our evaluation. Another significant source is provided by the Forties 5, which we estimate to

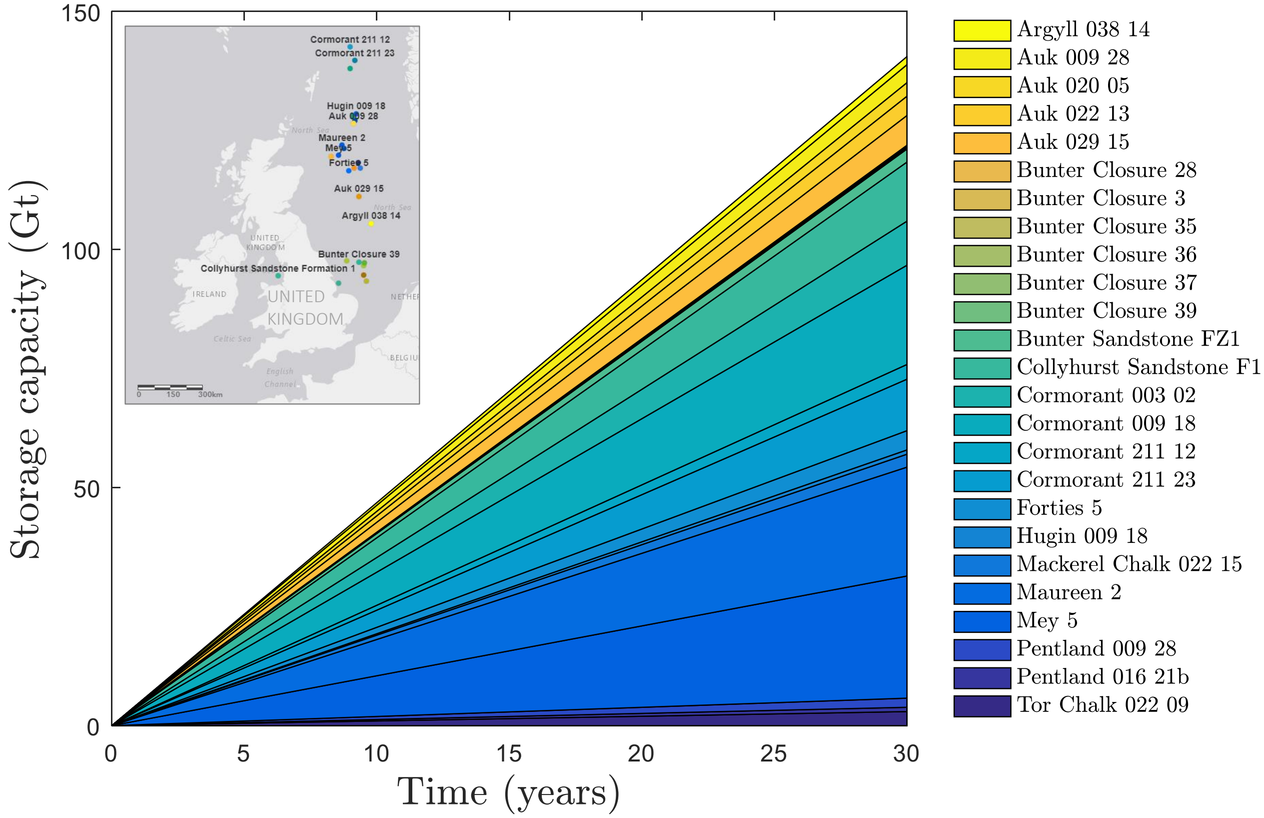

Figure 9: Maximum storage capacity of the selected UK sites for 30 years of continuous injection and maximum well number equal to 200.

be able to store 4 Gt in 30 years using 196 injectors.

For the Bunter Sandstone Formation 1 we estimate a maximum storage of 2.74 Gt, which is achieved by injecting CO_2 into 144 wells placed at a spacing of 6 km. The storage capacity is not dissimilar (2.6 Gt) if we inject into 42 wells (see Table S1 in Supporting Information). For the same region and timescale Heinemann et al. (2012) estimate a greater storage capacity, 7.8 Gt. The different estimates may be explained as a consequence of two major discrepancies. On the one hand, the authors use a formation area nearly a factor of 10 greater than in this study (56 660km^2 vs 5 126km^2). Countering this, however, Heinemann et al. (2012) approximate the overpressure by means of numerical simulation of single well injection into a closed domain with radius equal to half the interwell distance. This incurs an overestimation of the overpressure. In contrast, Noy et al. (2012) perform multiwell numerical simulations in a 3D domain and find that just 1 Gt can be stored in the Bunter Sandstone Formation by injecting into 12 locations for 50 years. The discrepancy may be related with the adoption of different mechanical parameters or failure criteria, or with limiting the number of wells to 12, as the use of numerical simulations hinders the exploration of a large number of scenarios.

The Pale Blue Dot Energy (2016) report estimates a storage resource in the Bunter Closure 36 of 280 $MtCO_2$ with injection over 40 years. For this site we estimate a lower potential, with a value of 90 Mt stored in 30 years. We think the discrepancy is clerical. The

Table 2: Maximum storage capacity, per well injectivity and corresponding scenario of number of wells n and interwell distance d for each of the selected UK sites. We consider 30 years of continuous injection and a maximum of 200 wells.

Site name	V_M **(Gt)**	Q_M **(Mt/yr)**	d **(km)**	n
Argyll 038 14	1.70	0.29	6.0	196
Auk 009 28	3.77	0.64	4.2	196
Auk 020 05'	2.85	0.48	4.0	196
Auk 022 13	4.05	0.69	6.8	196
Auk 029 15	6.25	1.06	7.5	196
Bunter Closure 28	0.20	3.32	8.8	2
Bunter Closure 3'	0.08	1.29	5.1	2
Bunter Closure 35	0.18	3.02	7.3	2
Bunter Closure 36	0.09	1.53	4.9	2
Bunter Closure 37	0.13	2.09	5.3	2
Bunter Closure 39	0.12	2.03	4.9	2
Bunter Sandstone FZ1	2.74	0.63	6.0	144
Collyhurst Sandstone F1	12.41	3.76	6.2	110
Cormorant 003 02	9.26	3.43	3.8	90
Cormorant 009 18	20.84	3.55	2.9	196
Cormorant 211 12	3.10	1.43	2.5	72
Cormorant 211 23	10.81	2.13	3.6	169
Forties 5	4.04	0.69	8.3	196
Hugin 009 18	0.90	5.00	7.0	6
Mackerel Chalk 022 15	2.72	0.50	3.8	182
Maureen 2	22.87	3.89	13.3	196
Mey 5	25.65	4.70	11.4	182
Pentland 009 28	1.92	1.77	4.5	36
Pentland 016 21b	0.90	2.50	6.2	12
Tor Chalk 022 09	2.95	0,50	4,2	196

parameters reported in the report, as well as the aquifer surface area, appear more similar to the values of Formation 4 comprising closure units 35, 36, 37, and 39. The cumulative storage that we evaluate for the Bunter Closures 35, 36, 37 and 39 is around 500 Mt.

A detailed site characterization is not usually available and there are significant uncertainties in the storage resource estimates. The greatest uncertainty is related to the geomechanical parameters, which are often difficult to estimate. Given the lack of information about these parameters in the CO_2 stored database, we explore here the sensitivity of the storage capacity to the values of the geomechanical parameters by assuming a range of possible values. The ratio of the average horizontal stress to the vertical stress, $\overline{\sigma_h'}/\sigma_v$, varies over a range between 0.5 and 2 (Brown and Hoek, 1978). Values smaller than 1 correspond to the case of a normal faulting regime (extensional), whereas values greater than 1 correspond to a reverse faulting regime (compressional). Values of the friction angle, φ, vary between 25° and 35° (Jaeger et al., 2009). We vary cohesion, C, from 0 up to 10 MPa. The lower value corresponds to the presence of pre-existing faults, the upper to the case of a well-compacted rock. We also consider the uncertainty of the permeability, κ, by increasing and decreasing the reference value for each site, κ^*, by one order of magnitude.

Figure 10 shows the variation of the total storage capacity with the values of parameters considered. Storage capacity increases with C and φ as the limiting overpressure increases, reflective of an increasing strength of the rock. A similar increase in the limiting overpressure, and thus storage capacity, is observed with increasing $\overline{\sigma_h'}/\sigma_v$. This represents an increase in the *in situ* average stress, as the vertical stress is fixed, and moves the stress condition away from the failure condition. The response is more sensitive to the stress ratio $\overline{\sigma_h'}/\sigma_v$ than to the strength parameters. A reduction of $\overline{\sigma_h'}/\sigma_v$ from 0.7 to 0.5 means a loss of storage capacity greater than 50%. The response is also very sensitive to permeability, which affects the overpressure response to the injection. An increase in permeability of one order of magnitude results in a reduction of the overpressure such that the total storage increases by almost 70%. Overall, the range of plausible system parameters results in a variation in injectivity from 0.8 - 8.6 Gt y^{-1} around the baseline of 4.7 Gt y^{-1}.

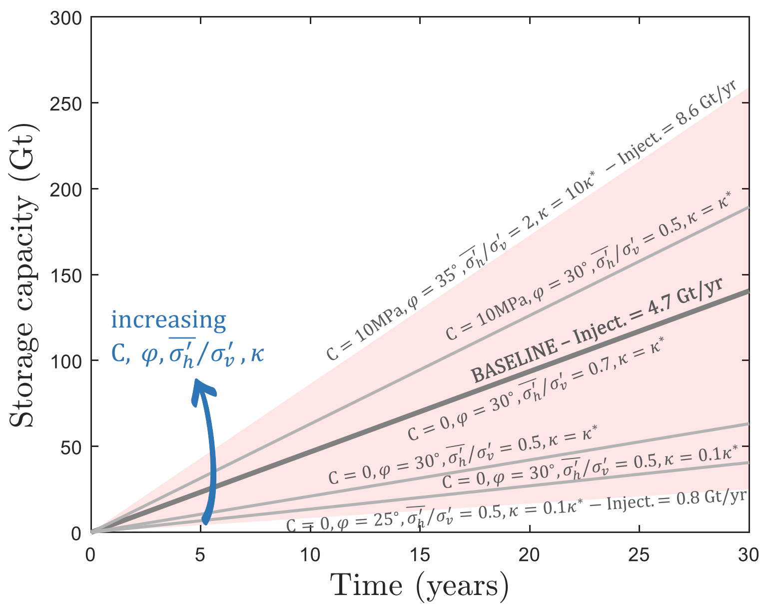

Figure 10: Uncertainty of the total UK storage resource for 30 years of continuous injection and a maximum of 200 wells per site. We explore the impact of changing the permeability, κ, and the geomechanical parameters, such as the cohesion, C, the ratio of the average horizontal stress to the vertical stress, $\overline{\sigma_h'}/\sigma_v$, and the friction angle, φ.

3.2 Optimising storage resource use for revenue

We now provide a simple example of the use of CO2BLOCK for the economic optimization of site use. Given revenues associated with CO_2 disposal and costs associated with well construction, we evaluate the tradeoff between cost and revenue for different scenarios of well numbers in the Bunter Closure 28 and Forties 5 sites. For each well number scenario, we consider the maximum allowable well distance (close to the red lines in Figure 8), which maximizes the storage.

Following Carneiro et al. (2015) and Mathias et al. (2015), the storage cost in deep offshore saline formations is calculated as the sum of the following components: drilling cost = k€26 per meter length of well, fixed cost per well = k€8200 per well, cost for the surface facilities on the injection sites = k€6120 per well, cost of site development = k€24 097, and cost of monitoring equipment = k€1530, plus a 5% for additional operating, maintenance, and monitoring costs. A cost of 50 €tCO_2^{-1} for capture costs is assumed, but this can range widely (Rubin et al., 2015; IPCC, 2005). Transportation cost ranges between 1-8 €tCO_2^{-1} for a pipeline of 250 km, depending on the terrain conditions and whether the pipeline is onshore or offshore (IPCC, 2005). A total value of 10 €tCO_2^{-1} is assumed for both sites. We disregard the presence of existing oil and gas infrastructure and facilities that might be re-employed, with consequent cost reduction. For the revenue, five scenarios are considered with revenue between 5 and 200 €tCO_2^{-1}, reflecting values from simple tax credits to revenues from enhanced oil recovery (Kolster et al., 2017). Detailed equations and a summary table are provided in Supporting Information, Section S6.

The investment cost, the sum of transport, capture and storage costs, is usually dominated by the capture and transportation cost, which increases linearly with the injected volume. However, storage costs can be significant for scenarios with large numbers of wells providing marginal enhancement in injectivity (see Figures S3C and S4C in Supporting Information). Revenue also increases linearly with the injected volume (Supporting Information, Figs. S4D and S3D), and thus net revenue (the difference between revenue and cost) mostly depends linearly on the total injected volume and the difference between the tax revenue and the sum of capture and transport costs (Fig. 11). For 30 years of injection, the transport and capture costs dominate and most of the fields in this example become profitable at a CO_2 incentive of 70 €tCO_2^{-1}.

In the case of the Forties 5, the net revenue is monotonic with the number of wells; once a threshold CO_2 incentive is provided, the project is most profitable with around 200 injection sites. In the case of the Bunter Closure 28, the net revenue is maximised with two wells. The behavior is a consequence of the variation of the storage capacity with the number of wells. In the case of the Forties 5, the storage capacity monotonically increases with the number of wells until reaching a plateau for $n > 200$, where the storage capacity oscillates around a constant value (Supporting Information, Fig. S3A and B). Net revenue follows the same trend but it diverges for large well numbers, where the impact of the storage cost on the total cost is greater. As a consequence, the maximum revenue corresponds to an intermediate number of wells. The behavior is similar for the Bunter Closure 28, but in this case both the maximum capacity and the maximum net revenue are achieved with two wells placed at very large distance (Supporting Information, Fig. S4A and B).

This is a simple example, intended to be illustrative, of the use of this tool in considering financial analysis of storage resource development. Far more sophisticated models could as easily make use of the underlying representation of storage resource use provided by CO2BLOCK, e.g., accounting for more infrastructure components and operational costs and financial issues like depreciation, borrowing, and insurance costs.

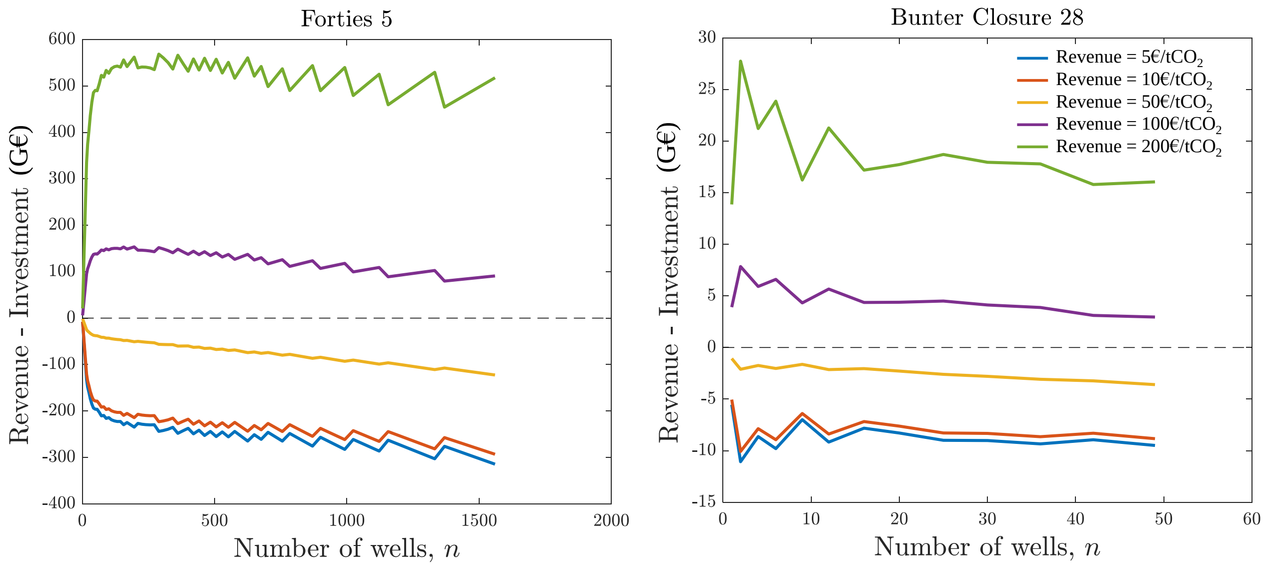

Figure 11: Net revenue (revenues minus investment) for the Forties 5 (left) and the Bunter Closure 28 (right) sites calculated by means of a simplified economic analysis. We assume the case of 30 years of continuous injection under different scenarios of well numbers and revenue values.

4 Discussion and Conclusions

In this paper we have presented CO2BLOCK, a tool for the preliminary evaluation of the CO_2 storage potential of geologic formations under different configurations of well numbers and distance. The procedure reflects the dynamic nature of pressure limitations on storage resource use, which provides a more realistic storage resource assessment than the static estimates (Zhou et al., 2008; Bachu et al., 2007; Bachu, 2015), adopted by other storage simulator tools (e.g., Burruss et al., 2009; Brennan et al., 2010; Poulsen et al., 2014; Gorecki et al., 2009). The simultaneous injection into multiple wells is an efficient strategy for pressure management and our tool analyses different multiwell scenarios with the pressure build-up evaluated as the superposition of single-well analytic models. This approach is also adopted in a similar software, EasiTool (Ganjdanesh and Hosseini, 2017, 2018), but CO2BLOCK includes a correction factor for the superposition error. From the output, optimisation may be performed, for example, to consider tradeoffs between costs and maximising injection volumes in a storage resource.

We demonstrate the use of CO2BLOCK to perform an estimate of the maximum storage resource in the UK offshore system, including an uncertainty analysis. Neglecting consideration of any regulatory and economic constraints, we estimate that around 140 Gt of CO_2 can be safely stored in 30 years through injection into 25 sites in UK identified through a screening for advantageous reservoir properties. Uncertainty from leading order geological parameters alone result in an order of magnitude range in the estimate, from 25 - 250 Gt of resource potential.

We also present a simple example of using CO2BLOCK for the economic optimization of site use. The design of this tool is intended to allow for the optimization of site development in more complex techno-economic energy models so that they may identify possible limitations in the deployment of CCS from injectivity and geography.

Although subject to simplifications, this rapid, yet accurate, estimate of storage capacities is ideal for a first screening process at the basin or regional scale. The accuracy of the solution under different scenarios of parameters depends on the sensitivity of the adopted analytical model (Nordbotten et al. (2005) - see also the discussion in Vilarrasa et al. (2010)) and on the superposition correction. De Simone et al. (2019) show that this approach provides accurate predictions under typical parameter values. The impossibility to reproduce heterogeneity is compensated by the possibility of performing sensitivity and uncertainty analysis around all the parameters in a reasonable computation time. However, more advanced analyses of the resource at the reservoir scale require the use of numerical simulations with a more complex and detailed reconstructed geological domain.

Acknowledgements

The authors acknowledge financial support from the MESMERISE-CCS (Multi-scale Energy Systems Modelling Encompassing Renewable, Intermittent, Stored Energy and Carbon Capture and Storage - EP/M001369/1) and the UKCCSRC 2017 (UK Carbon Capture and Storage Research Centre 2017 - EP/P026214/1) projects funded by the Engineering and Physical Sciences Research Council (EPSRC). All data are detailed in the manuscript or in the Supporting Information. CO2BLOCK is available at the repository https://github.com/co2block/CO2BLOCK or at http://doi.org/10.5281/zenodo.4313311).

References

Akimoto, K., Tomoda, T., Fujii, Y., and Yamaji, K. (2004). Assessment of global warming mitigation options with integrated assessment model DNE21. *Energy Econ. 26 (4), 635-653.*

Azizi, E. and Cinar, Y. (2013). Approximate Analytical Solutions for CO2 Injectivity Into Saline Formations. *SPE Reservoir Evaluation & Engineering*, 16(2):123–133.

Bachu, S. (2008). CO2 storage in geological media: Role, means, status and barriers to deployment. *Progress in Energy and Combustion Science*, 34(2):254–273.

Bachu, S. (2015). Review of CO2 storage efficiency in deep saline aquifers. *International Journal of Greenhouse Gas Control*, 40:188–202.

Bachu, S., Bonijoly, D., Bradshaw, J., Burruss, R., Holloway, S., Christensen, N. P., and Mathiassen, O. M. (2007). CO2 storage capacity estimation: Methodology and gaps. *International journal of greenhouse gas control*, 1(4):430–443.

Bentham, M., Mallows, T., Lowndes, J., and Green, A. (2014). CO2 STORage Evaluation Database (CO2 stored). the UK's online storage atlas. *Energy Procedia*, 63:5103–5113.

Brennan, S. T., Burruss, R. C., Merrill, M. D., Freeman, P. A., and Ruppert, L. F. (2010). A probabilistic assessment methodology for the evaluation of geologic carbon dioxide storage. *US Geological Survey Open-File Report*, 1127(2010):31.

Brown, E. T. and Hoek, E. (1978). Trends in relationships between measured in-situ stresses and depth. *International Journal of Rock Mechanics and Mining Sciences & Geomechanics Abstracts*, 15(4):211–215.

Burruss, R. C., Brennan, S. T., Freeman, P. A., Merrill, M. D., Ruppert, L. F., Becker, M. F., Herkelrath, W. N., Kharaka, Y. K., Neuzil, C. E., Swanson, S. M., et al. (2009). Development of a Probabilistic Assessment Methodology for Evaluation of Carbon Dioxide Storage U.S. Geological Survey Open-File Report 2009–1035, 81 p.

Carneiro, J., Martinez, R., Suaréz, I., Zarhloule, Y., and Rimi, A. (2015). Injection rates and cost estimates for CO2 storage in the west mediterranean region. *Environmental earth sciences*, 73(6):2951–2962.

Chandler, M. R., Meredith, P. G., Brantut, N., and Crawford, B. R. (2016). Fracture toughness anisotropy in shale. *Journal of Geophysical Research: Solid Earth*, 121(3):1706–1729.

De Simone, S., Jackson, S. J., and Krevor, S. (2019). The error in using superposition to estimate pressure during multi-site subsurface CO2 storage. *Geophysical Research Letters*, 46(12):6525–6533.

Dentz, M. and Tartakovsky, D. M. (2009). Abrupt-interface solution for carbon dioxide injection into porous media. *Transport in Porous Media*, 79(1):15–27.

Ellsworth, W. L. (2013). Injection-induced earthquakes. *Science*, 341(6142):1225942–1225942.

Energy Technologies Institute LLP, E. (2018). CO2stored database. http://www.co2stored.co.uk/.

Gammer, D., Green, A., Holloway, S., and Smith, G. (2011). The Energy Technologies Institute's UK CO2 storage appraisal project (UKSAP).

Ganjdanesh, R. and Hosseini, S. A. (2017). Geologic Carbon Storage Capacity Estimation Using Enhanced Analytical Simulation Tool (EASiTool). *Energy Procedia*, 114(November 2016):4690–4696.

Ganjdanesh, R. and Hosseini, S. A. (2018). Development of an analytical simulation tool for storage capacity estimation of saline aquifers. *International Journal of Greenhouse Gas Control*, 74:142–154.

Global CCS Institute, G. (2017). The global status of CCS: 2017 report. *Australia.*

Gorecki, C. D., Sorensen, J. A., Bremer, J. M., Knudsen, D., Smith, S. A., Steadman, E. N., Harju, J. A., et al. (2009). Development of storage coefficients for determining the effective CO2 storage resource in deep saline formations. *SPE International Conference on CO2 Capture, Storage, and Utilization.*

Heinemann, N., Wilkinson, M., Pickup, G. E., Haszeldine, R. S., and Cutler, N. A. (2012). CO2 storage in the offshore UK Bunter Sandstone Formation. *International Journal of Greenhouse Gas Control*, 6:210–219.

Herzog, H. J. (2011). Scaling up carbon dioxide capture and storage: From megatons to gigatons. *Energy Economics*, 33(4):597–604.

Huang, X., Bandilla, K. W., Celia, M. A., and Bachu, S. (2014). Basin-scale modeling of CO2 storage using models of varying complexity. *International Journal of Greenhouse Gas Control*, 20:73–86.

IEA (2017). Energy technology perspectives 2017. *International Energy Agency.*

IPCC (2005). IPCC special report on carbon dioxide capture and storage. prepared by working group III of the Intergovernmental Panel on Climate Change. *In: Metz, B., Davidson, O., de Coninck, H.C., Loos, M., Meyer, L.A. (eds.). Cambridge University Press, Cambridge, United Kingdom and New York, NY, USA, 442 pp.*

IPCC (2018). IPCC special report on global warming of 1.5ºC.

Jaeger, J. C., Cook, N. G., and Zimmerman, R. (2009). Fundamentals of rock mechanics. *John Wiley & Sons.*

Joshi, A., Gangadharan, S., and Leonenko, Y. (2016). Modeling of pressure evolution during multiple well injection of CO2 in saline aquifers. *Journal of Natural Gas Science and Engineering*, 36:1070–1079.

Koelbl, B. S., van den Broek, M. A., Faaij, A. P. C., and van Vuuren, D. P. (2014). Uncertainty in carbon capture and storage (CCS) deployment projections: a cross-model comparison exercise. *Climatic Change*, 123(3-4):461–476.

Kolster, C., Masnadi, M. S., Krevor, S., Mac Dowell, N., and Brandt, A. R. (2017). CO2 enhanced oil recovery: a catalyst for gigatonne-scale carbon capture and storage deployment? *Energy & Environmental Science*, 10(12):2594–2608.

Krevor, S., Blunt, M., Trusler, J., and De Simone, S. (2019). An introduction to subsurface CO2 storage. In *Carbon Capture and Storage*, pages 238–295. Royal Society of Chemistry.

Mathias, S. A., de Miguel, G. J. G. M., Thatcher, K. E., and Zimmerman, R. W. (2011). Pressure Buildup During CO_2 Injection into a Closed Brine Aquifer. *Transport in Porous Media*, 89(3):383–397.

Mathias, S. A., Gluyas, J. G., Goldthorpe, W. H., and Mackay, E. J. (2015). Impact of maximum allowable cost on CO2 storage capacity in saline formations. *Environmental science & technology*, 49(22):13510–13518.

Mathias, S. A., Hardisty, P. E., Trudell, M. R., and Zimmerman, R. W. (2009). Approximate Solutions for Pressure Buildup During CO2 Injection in Brine Aquifers. *Transport in Porous Media*, 79(2):265–284.

National Academy of Science (2012). Induced Seismicity Potential in Energy Technologies.

Neufeld, J. A., Hesse, M. A., Riaz, A., Hallworth, M. A., Tchelepi, H. A., and Huppert, H. E. (2010). Convective dissolution of carbon dioxide in saline aquifers. *Geophysical research letters*, 37(22).

Nordbotten, J. M., Celia, M. A., and Bachu, S. (2005). Injection and Storage of CO2 in Deep Saline Aquifers: Analytical Solution for CO2 Plume Evolution During Injection. *Transport in Porous Media*, 58(3):339–360.

Noy, D., Holloway, S., Chadwick, R., Williams, J., Hannis, S., and Lahann, R. (2012). Modelling large-scale carbon dioxide injection into the Bunter Sandstone in the UK southern north sea. *International Journal of Greenhouse Gas Control*, 9:220–233.

Pale Blue Dot Energy, R. (2016). Progressing development of the UK's strategic carbon dioxide storage resource. a summary of results from the strategic UK CO2 storage appraisal project. *Pale Blue Dot Energy.*

Peduzzi, P. and Harding Rohr Reis, R. (2013). Gas fracking: can we safely squeeze the rocks? *Environmental Development*, 6:86–99.

Poulsen, N., Holloway, S., Neele, F., Smith, N. A., and Kirk, K. (2014). CO2StoP Final Report Assessment of CO2 storage potential in Europe. European Commission Contract No ENER/C1/154-2011-SI2.611598 .

Ringrose, P. and Oldenburg, C. (2018). Mission innovation task force reports on enabling gigatonne-scale CO2 storage. *First Break*, 36(7):67–72.

Rubin, E. S., Davison, J. E., and Herzog, H. J. (2015). The cost of CO2 capture and storage. *International Journal of Greenhouse Gas Control*, 40:378–400.

Rutqvist, J. (2012). The geomechanics of CO2 storage in deep sedimentary formations. *Geotechnical and Geological Engineering*, 30(3):525–551.

Rutqvist, J., Birkholzer, J., and Tsang, C.-F. (2008). Coupled reservoir–geomechanical analysis of the potential for tensile and shear failure associated with CO2 injection in multilayered reservoir–caprock systems. *International Journal of Rock Mechanics and Mining Sciences*, 45(2):132–143.

Szulczewski, M. L., MacMinn, C. W., Herzog, H. J., and Juanes, R. (2012). Lifetime of carbon capture and storage as a climate-change mitigation technology. *Proceedings of the National Academy of Sciences*, 109(14):5185–5189.

Vilarrasa, V., Bolster, D., Dentz, M., Olivella, S., and Carrera, J. (2010). Effects of CO2 Compressibility on CO2 Storage in Deep Saline Aquifers. *Transport in Porous Media*, 85(2):619–639.

Vilarrasa, V. and Carrera, J. (2015). Reply to Zoback and Gorelick: Geologic carbon storage remains a safe strategy to significantly reduce CO2 emissions. *Proceedings of the National Academy of Sciences*, 112(33):E4511–E4511.

Zakrisson, J., Edman, I., Cinar, Y., et al. (2008). Multiwell injectivity for CO2 storage. *SPE Asia Pacific Oil and Gas Conference and Exhibition*.

Zhou, Q. and Birkholzer, J. T. (2011). On scale and magnitude of pressure build-up induced by large-scale geologic storage of CO2. *Greenhouse Gases: Science and Technology*, 1(1):11–20.

Zhou, Q., Birkholzer, J. T., Tsang, C.-F., and Rutqvist, J. (2008). A method for quick assessment of CO2 storage capacity in closed and semi-closed saline formations. *International Journal of Greenhouse Gas Control*, 2(4):626–639.

Zoback, M., Barton, C., Brudy, M., Castillo, D., Finkbeiner, T., Grollimund, B., Moos, D., Peska, P., Ward, C., and Wiprut, D. (2003). Determination of stress orientation and magnitude in deep wells. *International Journal of Rock Mechanics and Mining Sciences*, 40(7-8):1049–1076.

Zoback, M. D. and Gorelick, S. M. (2012). Earthquake triggering and large-scale geologic storage of carbon dioxide. *Proceedings of the National Academy of Sciences*, 109(26):10164–10168.